Applied Surface Science 263 (2012) 174–181

Contents lists available at SciVerse ScienceDirect

Applied Surface Science

journal homepage: www.elsevier.com/locate/apsusc

Verification of surface polarity of O-face ZnO(0 0 0 $\bar{1}$) by quantitative modeling analysis of Auger electron spectroscopy

C.W. Su*, M.S. Huang, T.H. Tsai, S.C. Chang

Department of Electrophysics, National Chiayi University, 300 Syuefu Rd., Chiayi 60004, Taiwan

ARTICLE INFO

Article history:
Received 10 August 2012
Received in revised form 2 September 2012
Accepted 8 September 2012
Available online 15 September 2012

Keywords:
Structure of clean surfaces
Polarity surfaces
Quantitative spectra analysis
Auger electron spectroscopy

ABSTRACT

Is crystalline ZnO(0 0 0 $\bar{1}$) O-face surface believed to be enriched by Zn atoms? This study may get the answer. We proposed a simplified model to simulate surface concentration ratio on (0 0 0 $\bar{1}$)-O or (0 0 0 1)-Zn surface based on the hard-sphere model. The simulation ratio was performed by integrating electron signals from the assumed Auger emission, in which the electron mean free path and relative atomic layer arrangements inside the different polarity ZnO crystal surface were considered as relevant parameters. After counting more than 100 experimental observations of Zn/O ratios, the high frequency peak ratio was found at around 0.428, which was near the value predicted by the proposed model using the IMFP database. The ratio larger than the peak value corresponds to that observed in the annealed samples. A downward trend of the ratio evaluated on the post-sputtering sample indicates the possibility of a Zn-enriched phase appearing on the annealed O-face surface. This phenomenon can further elucidate the O-deficiency debate on most ZnO materials.

1. Introduction

The performance of optoelectronic devices is unsatisfactory due to high dislocation density from large surface/interface lattice mismatch between the substrate and epitaxial layer. Therefore, understanding how to obtain a high quality substrate surface is the key for further processing. ZnO is a known material with a wide band gap of 3.37 eV at room temperature, has high excitonic binding energy of 60 meV, and has the advantages to operate near soft ultraviolet wavelength regions [1–7]. Although topics about ZnO in the academic field have been discussed for over five decades, ZnO still has excellent optoelectronic properties for device applications that need to be explored. With the rapid advancement in nanotechnology and precise control in thin film processing, ZnO has become an excellent candidate material for the development of new generation devices.

However, the ZnO surface have the worse conditions before any processing, such as scratches from mechanical polishing and large concentration of defects or domain islands in a single crystal surface [8,9]. Therefore, thermal annealing at high temperature is an essential procedure to flatten the surface to reduce the rough surface condition. The uncertain surface state of composite materials such as silicon carbide controls further the material processing and properties [10]. *c*-axis ZnO has two distinct polar faces, namely, (0 0 0 1) Zn- and (0 0 0 $\bar{1}$) O-faces. The polarity of ZnO films is difficult to control because ZnO films on sapphire usually have O-polarity; intrinsic oxygen vacancies and interstitial zinc atoms also exists in most n-type ZnO semiconductors [11,12]. A thermal treatment substantially improves the surface of both O- and Zn-face ZnO, making them appropriate for further epitaxy. The atomic force microscopy (AFM) results showed terrace-like features after annealing at 1050 °C at either the Zn-face (Zn-terminated) or O-face (O-terminated) surface [8]. However, the results still cannot completely explain most of the Zn atoms situated on the annealed Zn-face surface, and vice versa.

Two-dimensional (2D) growth is required to achieve stable p-type conductivity and precise device structures, such as quantum wells [11]. Although ZnO p-type semiconductor doping is difficult, p-type electronic configuration may be achieved by altering the O-face property rather than that of the Zn-face surface [13]. However, the correlation between the Zn/O ratio and material properties of O-polarity ZnO needs to be further clarified.

In this study, the Zn/O ratio was evaluated through Auger electron spectroscopy (AES), utilizing different sputtering conditions on the O-terminated surface, in which the sputtering energy varied from 300 eV to 2000 eV. Through post ratio analysis using the simplified hard-sphere and electron mean-free-path models, more evidences can be obtained to prove whether the surface belongs to the Zn- or O-type surface. Different faces may induce various physical and chemical properties. The film structure is dominated by the initial type of surface when the terminated atomic layer is different. Interestingly, a recent study indicated that either

* Corresponding author. Tel.: +886 5 2717905; fax: +886 5 2717909.
E-mail address: cwsu@mail.ncyu.edu.tw (C.W. Su).

0169-4332/$ – see front matter © 2012 Elsevier B.V. All rights reserved.
http://dx.doi.org/10.1016/j.apsusc.2012.09.023

Zn-polar nanowires or O-polar pyramids are observed on the $(0\,0\,0\,\bar{1})$ O-polar surface [13]. The surface condition in which the polarity is dominated is conducive to understand further the growth of nanostructures or thin films, such as different growth rates on opposite crystal polarities. In addition, O-face ZnO is more suitable for the production of high quality GaN epitaxial layers due to its low lattice mismatch [14]. Thus, this study focused on the O-terminated surface rather than the Zn-terminated surface.

Surface stoichiometry is especially affected by the surface treatment material constitution processing with more than two elements. In oxide or nitride semiconductors, i.e., the III-V or II-VI groups, structural defects and stoichiometry changes are easily introduced via ion bombardment and annealing [15]. Thus, sputtering is often used for substrate cleaning prior to thin film deposition. Energetic ion from discharging noble gases such as Ar^+ is typically used as a sputtering source. The sputtering accompanies surface composition variation. The surface composition of different ZnO surface terminations is deviated with low energy ion bombardment [16]. The Zn-face surface is more stable than the O-face because the Auger intensity ratio of Zn/O is not altered significantly with ion sputtering. The Zn content on the Zn-terminated ZnO surface is enriched relatively than that on the O-terminated surface. Moreover, obvious variation in sputtering ion energy occurs only at the O-face samples. However, these results still cannot point out the corresponding surface behavior from the top layer.

AES is a surface-sensitive technique based on the intense inelastic scattering that occurs for electrons in this energy range. Therefore, Auger electrons from only the outermost atom layers of a solid survive to be ejected and measured in the spectrum [17]. The whole chemical information near the surface region can be conveniently obtained by scanning the full spectrum. This study focuses on investigating the O-face ZnO(0 0 2) substrate surface because of its potential in optoelectronic and spintronics applications. The Zn-face ZnO surface is more chemical resistive and highly conductive than the O-face [16]. Several AES studies involve quantifying one or more adsorbates on an otherwise clean surface of one component [17]. ZnO$(0\,0\,0\,\bar{1})$ structure can be treated as one element covered on the other, e.g., the O atomic layer on the Zn-face ZnO is used as the O-terminated surface. Thus, the AES spectra analysis should be following the same quantification method in Ref. [17] as inhomogeneous thin or monoatomic overlayer samples. An empirical hard-sphere model is proposed to evaluate the AES measurement result. This study aims to analyze the different compositions of the ZnO surface that correspond to specific conditions after ion bombardment.

Ion-induced diffusion or segregation is complicated. Sputtering surface layers introduce considerable changes in surface stoichiometry, as well as the fundamental electric conductance in the semiconductor surfaces [18]. Stoichiometric 1:1 composition inside a clean bulk may be achieved after high-temperature annealing. However, ratio deviation may possibly occur in most of the top surface layers.

The electron inelastic-mean-free-path (IMFP) and effective-attenuation-length (EAL) models are commonly used for simulating the electron scattering trajectory in a material [19,20]. These models are often utilized to determine the overlayer thickness in Auger signal ratio analysis. The complete theoretical approach is described elsewhere [17]. In this study, the aforementioned models were used to compare the simulation of AES signals. The calculation result fits well with the ratio of the IMFP model than with the EAL model. When the empirical simulation was applied in this study, the statistical results of the ratios deviated significantly from our AES measurements, which may be attributed to the surface morphology altered by the dominant parameter of ion sputtering, i.e., the ion incident angle.

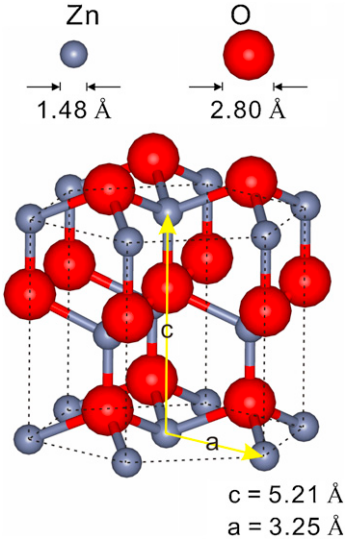

Fig. 1. Unit cell of a wurtzite ZnO(0 0 0 1) structure.

The main objective of this study is to propose a simple model to directly determine the surface polarity type of ZnO(0 0 0 1) through the quantitative analysis of the Auger signal ratios. With the advantage of surface sensitivity, AES is an accurate technique to measure the electron signal in the marked thin layer. After more than 100 observations in the last five years, the statistical ratios were demonstrated in a chart for modeling evaluation.

2. Experimental

The ZnO(0 0 0 1) crystal substrate created using a hydrothermal method was provided by Semiconductor Wafer, Inc. (Hsinchu, Taiwan). The specification of the crystal is as follows: size: $10 \times 10 \times 0.5 mm^3$; two-side polished; orientation tolerance: $\pm 0.5^\circ$; resistivity: 500 Ω-cm to 1000 Ω-cm. The lattice constant values of the wurtzite (hexagonal) structured ZnO are $a = 3.25$ and $c = 5.21$ Å [15,18]. The ion sizes of Zn^{2+} and O^{2-} based on the data of ionic radii are 1.48 and 2.80 Å, respectively [9,17,21]. The oxide plane shifted to 0.83 Å from the Zn plane along the *c*-axis [16]. The unit cell of a ZnO crystal structure according to the structural parameter is schemed in Fig. 1. The Miller-Bravais coordinate representation for the surface plane orientation is (0 0 0 1). After conversion from a 4-index system to 3-index scheme, the crystal plane of hexagonal ZnO surface is interpreted as (0 0 2) in most diffraction techniques.

The crystal was then treated with ultrasonic cleaner using ethanol, acetone, and deionized water before transferring into the ultrahigh vacuum (UHV) system. The UHV background pressure was 2×10^{-10} Torr. Approximately 2 keV/15 μA dc Argon plasma, generated by an ion source (Model: ISE-10, Omicron Technology Ltd.), was used to clean surface contaminations, typically, hydrocarbon, when the crystal was transferred into the UHV environment. The ion dose was estimated at 6.3×10^{16} ions/cm^2. Auger electron spectroscopy (SpectaLEED; Omicron Co. Ltd.) is equipped with a retarding field analyzer that detected electrons within a circular sector around 102° with primary incident beam energy at 3 keV. All measurements were conducted at room temperature.

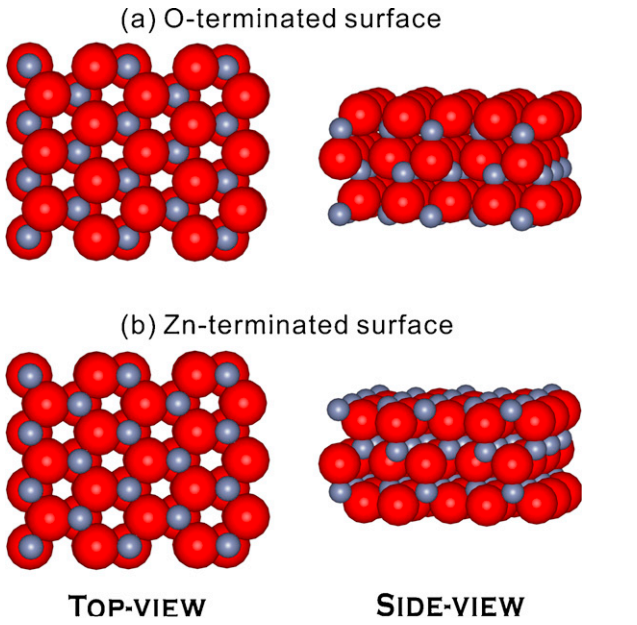

Fig. 2. Top-view (left column) and side-view (right column) representations of (a) an ideal O-terminated ZnO(0 0 2) surface structure and (b) an ideal Zn-terminated ZnO(0 0 2) surface structure.

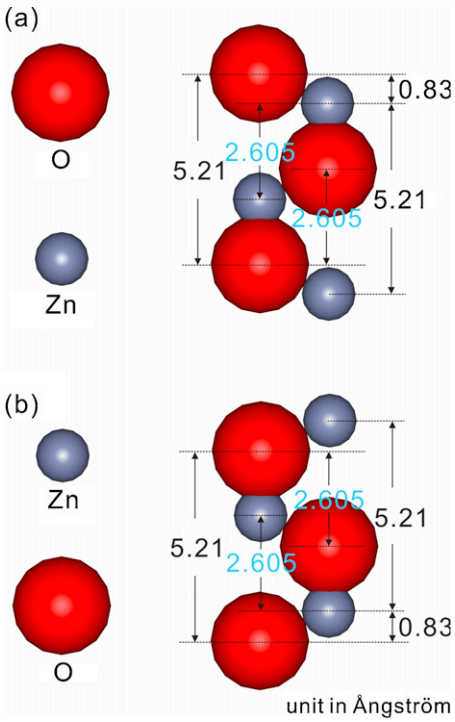

Fig. 3. Cross section of the atomic arrangement in a unit cell in (a) an O-terminated surface and (b) a Zn-terminated surface.

3. Results

The top and side views of the stacking of the O-face and Zn-face are shown in Fig. 2. The surface structure of an ideal O-face or O-terminated ZnO(0 0 0 $\bar{1}$) surface is terminated by oxygen, as shown in Fig. 2(a). According to the AFM image of the sample annealed at 1050 °C in the air, the surface morphology of the terrace-like O-face was different from that of the Zn-face [8]. A recent study reported that (0 0 0 1)-Zn and (0 0 0 $\bar{1}$)-O surfaces are not naturally stable because the internal dipole field inside the crystal is perfectly cleaved by polar surfaces [22]. However, most conductive ZnO films are originally oxygen deficient. According to related studies on $Co_xZn_{1-x}O$ diluted magnetic semiconductor films, one of the magnetic origin of the material may be attributed to oxygen vacancies [23]. The defect center is important in inducing exchange coupling. In the study, the structural property of the ZnO thin film is amorphous. Discussions on the magnetic-related issue of Co-doped ZnO, especially the ZnO(0 0 0 1) crystalline structure, are still controversial [24,25]. Thus, the O-rich phase ZnO(0 0 0 $\bar{1}$) surface was chosen to prevent the interference of O-defect to reduce the complexity of O-deficiency.

In this study, the Auger signal ratio is defined as the ratio of the peak height intensity of Zn to O. The ratio can be transformed into a concentration ratio by dividing it with a factor of 0.378 ($h^{Bulk}_{Zn_{LMM}}/h^{Bulk}_{O_{KLL}}$) [26]. The signal ratio simulation was based on the hard-sphere model, considering the depth-dependent electron mean free path. The theoretical signal ratio from the integration of each element signal was compared with the measured ratio of Zn to O. The simulation from Auger signal ratio calculation was completely based on a perfect atomic arrangement. The local surface relaxation or reconstruction, such as the occurrence of nano-pits, was not included in the simulation [22]. The Auger emission process is known as the specific secondary electron that leaves from the core level of the atom due to high-energy electrons that strike the atom within the surface region. Before escaping from the surface, the secondary electron penetrates several surface layers to the vacuum. These electrons in vacuum can be detected using a spectrometer. The proposed model is completely based on the classical collision with linear electron trajectory inside the atomic layer structure.

The approximate surface composition C_x for an element x in a compound can be expressed by as:

$$C_x = \frac{I_x}{S_x D_x} \Big/ \sum \frac{I_\alpha}{S_\alpha D_\alpha} \quad (1)$$

where I_x is the received electronic signal intensity for element x from the Auger signal analyzer; S_x, sometimes denoted as the peak-to-peak intensity I_x^∞ from the bulk, is the surface sensitivity of element x obtained from the AES handbook; and D_x is the instrumental variable from each AES equipment. Using the same condition in Eq. (1), D_x will be neglected from this formula.

Although the quantitative analysis of Eq. (1) is suitable for most amorphous compound, it does not work well in the estimation of an ideally crystal structure. Thus, the simulated AES signal ratio needs to be considered by the relative atomic layer arrangement of Zn and O in the z-axis [0 0 0 1] or [0 0 0 $\bar{1}$] direction. The schematic cross-section diagram containing only 6 atoms in a unit cell on the m-plane ZnO(10$\bar{1}$0) is divided into the O-face and Zn-face structures, as shown in the top and bottom of Fig. 3, respectively. The distances (listed in Fig. 3) between atomic layers are relevant parameters for further calculations. By integrating the signals, surface concentration may be recovered from the Auger peak-to-peak signal intensities.

The assumed hard-sphere models are shown in Fig. 4. An example of the O-face ZnO(0 0 0 $\bar{1}$) arrangement is presented. The received Auger signals cannot completely reflect the bulk information due to the surface sensitivity detected by the AES spectrometer only in a short surface regime, which is alternatively called selvage. Thus, the received Auger signal was limited by an atomic-dependent electron mean free path or attenuation length. Auger electrons scatter with atomic core in elastic and inelastic collisions until are emitted to vacuum. The key factor λ "lambda" on Fig. 4 is used to estimate the thickness measurement of an overlayer film

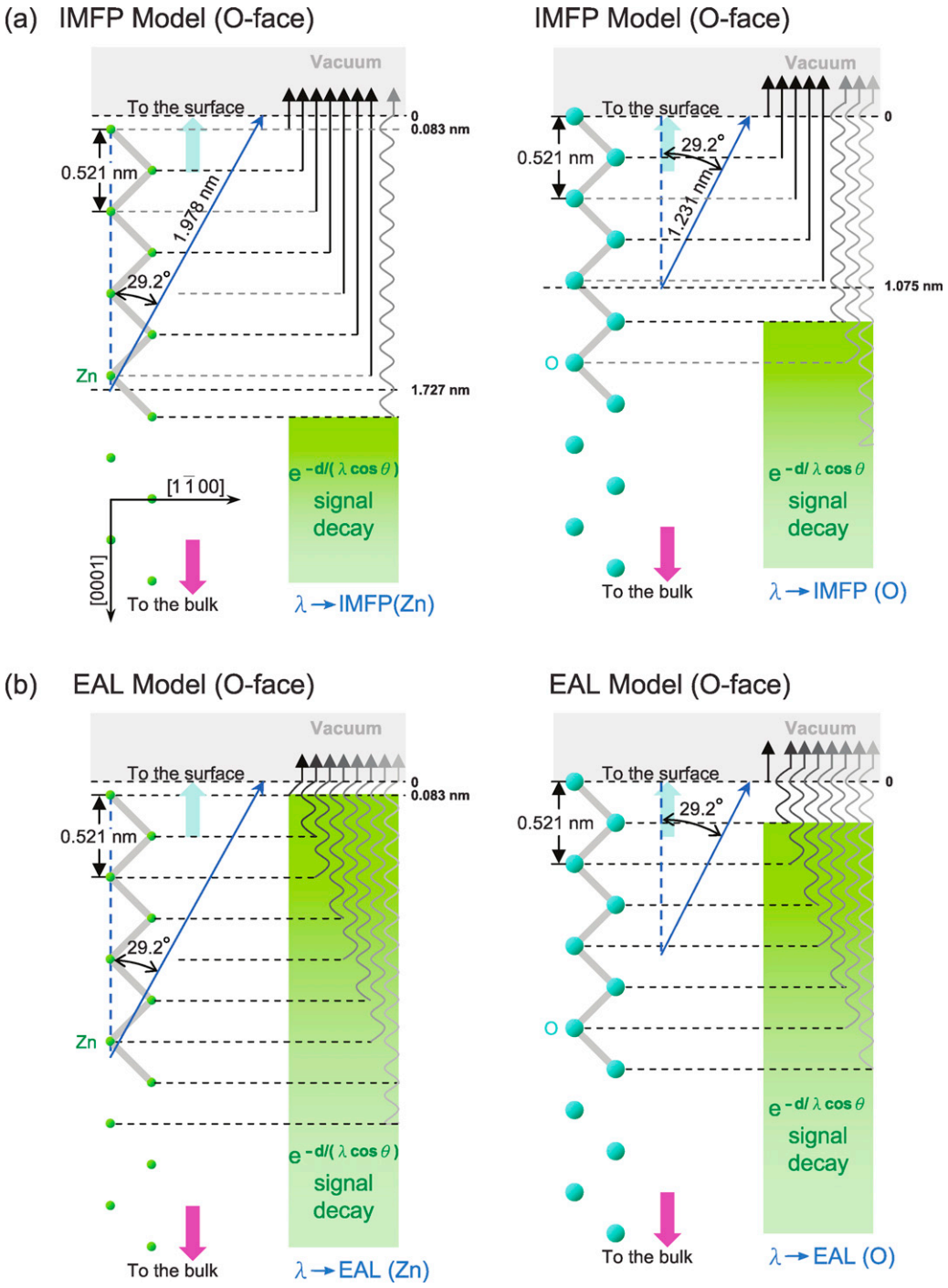

Fig. 4. (a) Simulated IMFP model of an O-face surface. (b) Simulated EAL model of an O-face surface. The left and right column figures correspond to the atomic arrangement of Zn and O, respectively. Detail of the calculation is described in the text.

or the depth measurement of a thin layer [17]. The λ value can be interpreted from two theoretical models, namely, IMFP and EAL. Each simulated model can be calculated and compared using the TPP-2M and Gries equations [27,28]. To date, λ values can easily be obtained from standard computer-based databases [19,20], similar to those given in Table 1.

The electronic signal was initially set to a condition that the electrons escape vertically without attenuation within the IMFP of Zn LMM (985 eV) transition, as shown in Fig. 4. However, the collection of Auger electrons in the retarding analyzer is spread over a sector within 102°. Thus, the corresponding λ value in the $[0\,0\,0\,\bar{1}]$ direction must be corrected to $\lambda\langle\cos\theta\rangle$. The $\langle\cos\theta\rangle$ is estimated using the equation: $\frac{180^\circ}{\pi\cdot 51^\circ}\int_0^{51^\circ}\cos\theta d\theta = 0.873$, to obtain the average emission angle $\overline{\theta} = \cos^{-1}0.873 = 29.2^\circ$. Therefore, the λ_z that projected in the z-axis has to be corrected to 1.727 nm according to the database (Fig. 4a). Noticeably, the IMFP database neglected the elastic scattering factor and only considered the inelastic scattering of Auger electrons. However, the EAL database included the effect of elastic scattering focused on the overlayer-film thickness and marker-layer (short range) depths. The EAL simulation consists of two material-dependent parameters: the IMFP and the transport mean free path (TMFP). The unique difference in our proposed model from the EAL is that the Auger signal is attenuated at

Table 1
Inelastic mean free path values (unit in nm) for the Zn LMM and O KLL main Auger transition peaks calculated using the TPP-2M and Gries equations.

	TPP-2M	Gries
E_g (eV)	3.37	
Zn(985 eV)	1.978	1.932
O(510 eV)	1.231	1.203

each layer in a depth-dependent function. Thus, the IMFP model simulation showed that λ_z exceeds the boundary or EAL beneath the surface, as denoted by the wave-like arrows in Fig. 4. The detail of the simulation of the Zn/O ratio is described in following two databases.

3.1. IMFP database

The IMFP data of the Zn LMM-transition (985 eV) and O KLL-transition (510 eV) transitions using the NIST IMFP database, calculated respectively with TPP-2M and Gries equations, are listed in Table 1. In the IMFP program, ZnO must be assigned as the inorganic compound instead of the individual Zn or O elemental database.

In the database program, the ZnO band gap was set at 3.37 eV; compound density was 5.606 g/cm^3; and the number of total valence electrons was 18 [16,19,29]. The stoichiometry coefficient for either Zn or O was set at 1 for a stoichiometric or a perfect crystal. According to the obtained result listed in Table 1, the shortest free path from the top layer surface is equal to the depth threshold calculated from $\lambda\bar{\theta}$, in which most Auger electrons escaped from the emission angle. The IMFP model represented, in which the Auger electrons can completely emit without scattering, is schemed in a cross section diagram (Fig. 4(a)). For example, Zn atom should be normalized as one atom signal when the layer structure depth from the center of the atom is located within the depth threshold obtained from IMFP. The elemental signal should then be counted because the Auger electron is emitted from the inner shell of the atomic energy level. The signal exponentially decays in a factor of $e^{-d/(\lambda\cos\theta)}$ when the path exceeds IMFP in the z-axis. The obvious difference in the layer staking of the O-face or Zn-face surface is the atom counted in the corresponding polarity surface. For example, the position of the topmost Zn layer for an O-terminated ZnO$(0\,0\,0\,\bar{1})$ should descend from the surface plane at 0.083 nm, with respect to the O plane. Therefore, the threshold depth of Zn electron increase 0.083 nm to 1.644 nm, indicating that seven Zn atoms with a length of three times that of a unit cell should be counted. According to the principle of the proposed model, the simulated model presented by the IMFP database can be simply be expressed as follows:

$$[\mathrm{Floor}(\frac{2\lambda\cos\bar{\theta}}{c})+1]+\sum_{n=1}\exp\{-[\mathrm{Floor}(\frac{2\lambda\cos\bar{\theta}}{c})+n+d']\cdot\frac{c}{2}/(\lambda\cos\bar{\theta})\} \quad (2)$$

where *Floor*[x] function provides the only integral part of x in the known MATHEMATICA© program or the same syntax in most statistical programs; λ is the IMFP obtained from the database, $\bar{\theta}$ is the average angle of the Auger electrons emitted with respect to the normal surface, which has been calculated in Section 3; c is ZnO lattice constant equal to 0.521 nm in the z-axis, and n is the nth atomic layer that starts to attenuate exponentially. d' in nm is 0.083, which was used to calculate the Zn signal and zero was used to calculate the O signal when the O-face was simulated. The d' value is reversed for a Zn-face surface. The Auger emission angle of 29.2° in our system is determined by the average of the received LEED/Auger screen, as described previously in Section 3. From Eq. (2), one atom signal is normalized by 1 when the layer position of the specific element is located within IMFP, which is lower than the lowest dashed line (the shortest distance in the z-projection of the IMFP), as shown in Fig. 4(a). Exceeding the boundary, the electron signal decays exponentially with depth (indicated as a shadow block and wave-like arrows).

3.2. EAL database

The EAL simulation in λ considers both elastic and inelastic scattering. The theoretical approach is based on the kinetic Boltzmann equation within the transport approximations [20]. Different from the IMFP model, the electron signal in the EAL model is depth-dependent, and always decays exponentially in addition to the topmost atomic layer at the surface. Except for the topmost electron denoted as a linear arrow, all electron signals attenuated. The schematic diagram is shown in Fig. 4(b). The EAL value is depth-dependent, thus, the signal integrated for the corresponding element is expressed as follows:

$$\sum\exp[-\frac{d+d'}{\lambda(d)}]=\sum_{n=1}\exp[-\frac{(n-1)c+d'}{2\lambda(d)}] \quad (3)$$

where d is the depth from the top surface; $\lambda(d)$ is the EAL value from the database and is dependent on the depth and emission angle; n is the nth layer from the top surface, c is the ZnO lattice constant, d' is 0.083 nm for the Zn signal and zero for O signals when the O-face is simulated. The d' value is reversed for a Zn-face surface. In the database program, 29° was set as the emission angle and 22° as the solid angle.

The normalized atomic signals based on the IMFP and EAL models from the $(0\,0\,0\,\bar{1})$-O terminated and $(0\,0\,0\,1)$-Zn terminated surfaces versus depth are shown in Fig. 5. The λ value in the calculations can be obtained using the TPP-2M or Gries equations in the NIST database. The atomic arrangement of the O-face or Zn-face is different during the estimation of atomic signals. The difference can be compared with the inlet schemes of Fig. 5(d) and (g). The Zn signal simulated by EAL length $\lambda(d)$ in the first top layer is attenuated by a factor of $e^{-0.083/\lambda(d)}$. The same process occurs in the opposite O-signal on the Zn-face surface. Fig. 5 shows that the atomic signal decays to zero when the equivalent depth was approximately 25 layer pairs (~7 nm) in the bulk region.

4. Discussions

Fig. 6 demonstrates the calculation result of the ratios versus the number of simulation layers using the two aforementioned models. The ratios were totally obtained by integrating signals from one layer pair to more than 50 layer pairs. The O-face and Zn-face simulation ratios with the simulation layers are shown in Fig. 6(a) and (b), respectively. In the AES principle, the simulation of more than 7 layer pairs is meaningless because most Auger signals for a perfect crystal originate from a relatively thick region, which is about only 6 atomic layer pairs in average [16]. Thus, a block region was labeled to obtain the average ratios located at about 0.428 in stoichiometric O-face ZnO$(0\,0\,0\,\bar{1})$ using the IMFP model and about 0.45 using the EAL model. For the Zn-face surface, the ratio increases to about 0.50 using the IMFP model and 0.51 using the EAL model. The convinced spectra and measured ratios from the as-received sample are shown with two polarities in Fig. 7. The simulation ratio using the IMFP model is in good agreement with the as-received experimental data. The experimental data collected in the statistical distribution of the Zn/O ratio is shown in Fig. 8. These data were obtained successively within the last five years, after more than 100 observations. The data in the former four years were obtained using different sputtering conditions without thermal annealing. Recently, the vacuum system can provide IR-heater facility for rapid annealing at

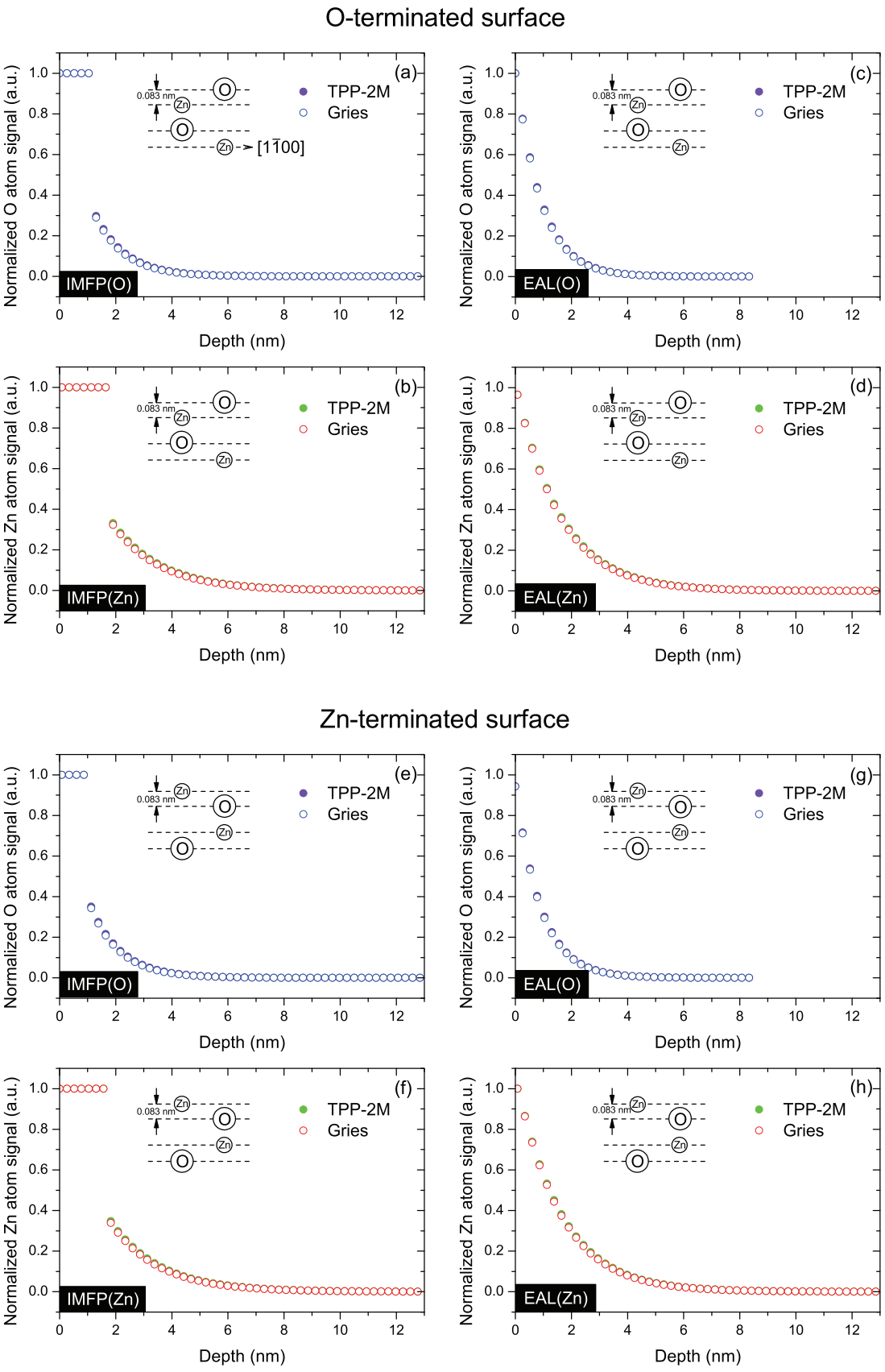

Fig. 5. Normalized Auger signals based on the model were calculated with depth in the [0 0 0 $\bar{1}$] direction on the O-face and [0 0 0 1] direction on the Zn-face. The database to simulate specific element in the proposed model is labeled at the bottom-left corner of each figure. Results (a) to (d) are simulated for an O-terminated surface, whereas (e) to (h) are simulated for a Zn-terminated surface. Each figure has two calculation results due to different simulation equations using the TPP-2M and Gries functions.

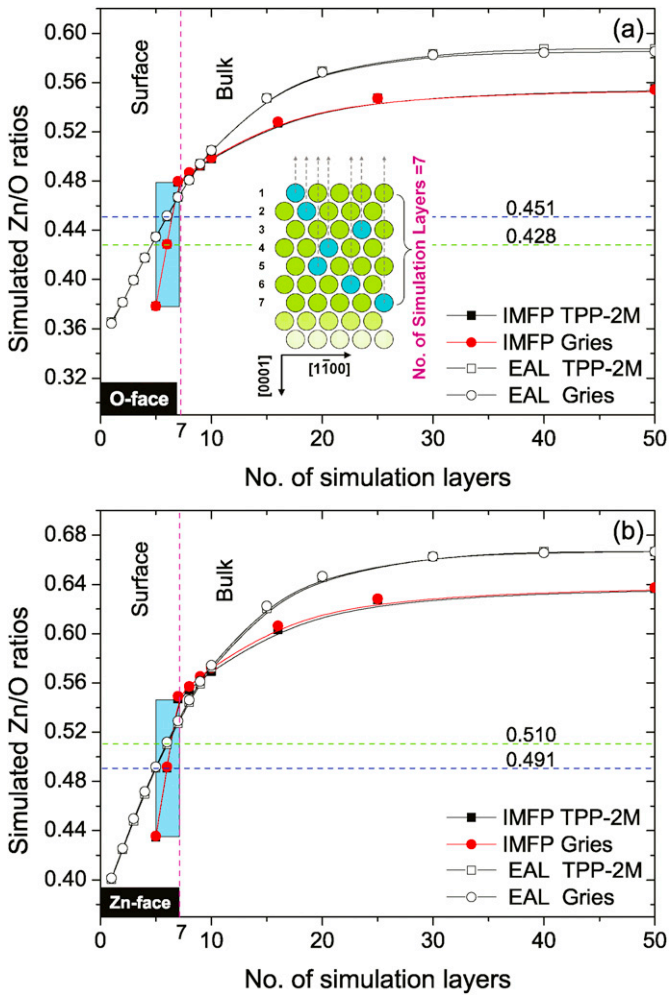

Fig. 6. Simulated Auger signal ratio was calculated versus the number of simulation layers up to 50 layer thick inside the ZnO. Due to the surface sensitivity of AES averaged from 5 to 7 layer pairs, the dash lines indicate that the average ratio is estimated at the ratio of the 6th layer using either the IMFP or EAL database. For example, the stoichiometric ratio using the IMFP model is 0.428±0.005 on an O-face surface and 0.491±0.005 on a Zn-face surface. According to the results from Fig. 5, four curves in (a) or (b) resulted from the simulation equations.

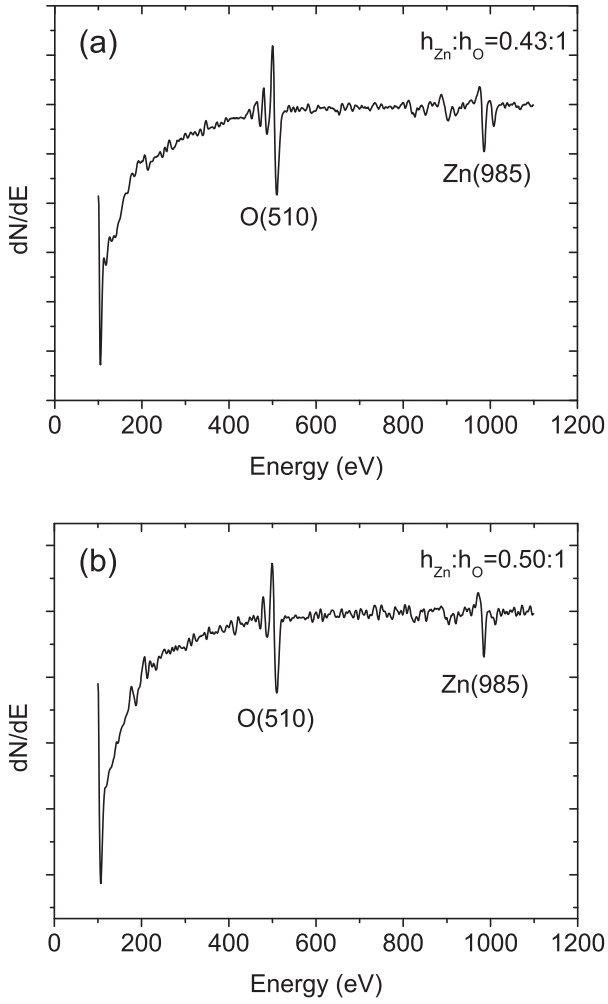

Fig. 7. Auger spectra of the as-received clean ZnO surface: (a) (0 0 0 $\bar{1}$) O-face and (b) (0 0 0 1) Zn-face. The peak height ratio indicated on the figures is well compared to our prediction value in Fig. 6.

about 500 °C for 10 min. Some annealing data were simultaneously included to observe the distribution of various ratios.

Fig. 8 shows that the fitted Gaussian curve in the statistical distribution exhibited three local peaks. The maximum peak at 0.428 is close to our prediction of stoichiometric phase using the IMFP model, and also corresponds to the condition that the O-face surface was sputtered by 1 keV to 2 keV dc Ar^+ ion sputtering. Every sample underwent normal sputtering for 30 min and oblique sputtering off the 60° angle at two sides for 15 min each. According to a related study, oblique sputtering is conducive for the generation of nano-patterning or locally flattening [30]. Another high frequency peak occurring at around 0.465 corresponds to the recent post-annealing condition. Moreover, the sputtering gas substituted to nitrogen also leads to a ratio greater than 0.428. The low ratio peak located at about 0.40 corresponds to the low energy of 0.5 keV to 0.75 keV Ar^+ sputtering. Therefore, the light N_2^+ ion sputtering leads to a Zn-rich phase rather than a heavier Ar^+ ion sputtering in the O-rich phase (shadow blocks in Fig. 8).

Although the simulated result fitted well with our prediction, the accuracy of the stoichiometric 1:1 ZnO ratio still needs to be confirmed. Most ZnO exhibited that O-deficiency exited in amorphous thin films. The statistical result also showed that the relative

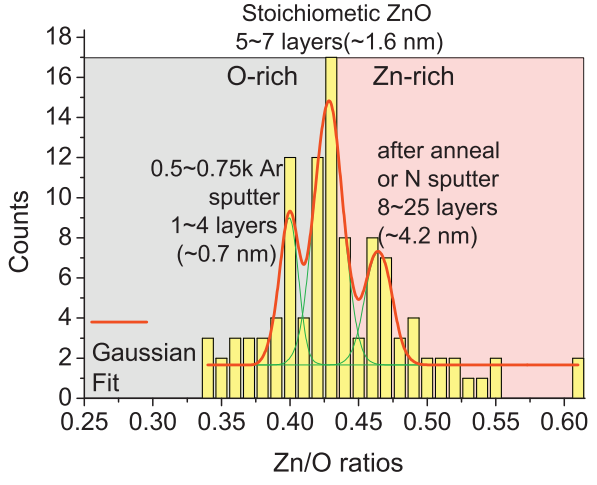

Fig. 8. The experimental Zn/O ratios measured in the recent five years are recorded in the statistical chart. Three peaks in the gaussian fit correspond well to the conditions of low-energy Ar^+ sputtering, stoichiometric, and high temperature annealing from left to right, respectively.

ratio is high after high temperature annealing. In other words, the same behavior also occurs in the ZnO(0 0 0 $\bar{1}$) crystalline structure because the relative Zn-rich phase may be generated after high temperature annealing. However, the inference only agrees with

the sputtering result, in which the number of O atoms is less than that in a bulk layer in the first double layer [16]. The ratios of the annealed sample were carefully compared with the sputtered sample. In the sputtering energy interval between 300 eV and 2000 eV, the ratio of the annealed sample decreased after Ar^+ sputtering, which was different from the conclusion in [16]. The opposite phenomenon may be attributed to the O-face surface enriched with Zn atoms. The surface Zn atoms on top of the annealed sample were sputtered by Ar^+ ions, leading to the decrease in ratios. This phenomenon is reasonable because the open SRIM program indicates that the sputtering yield of Zn is higher than O [31]. In addition, an initial O-face ZnO$(0\,0\,0\,\bar{1})$ may become a Zn-rich surface after high temperature annealing.

The results in the current study was compared with that of [16], in which the experimental Zn/O ratio on the O-face surface was approximately 0.62. The ratio from the proposed model deviated, especially at high-energy Auger peak. The large difference may be attributed to the glancing angle of ion incidence, which was approximately 86°, as indicated by [16]. Although oblique sputtering may not destroy the surface seriously, the result showed that the Zn/O ratio on the O-face was obviously larger than that on the Zn-face at the high-energy Auger peak. The published ratios are much higher than the result obtained using the IMFP and EAL models in this study. By contrast, our result can further infer the O-deficiency of the ZnO surface on the O-face surface. The results of this study are not perfect yet because related studies in microstructure are still in process. However, the simulation result of the average intensity ratio of Zn/O on the $(0\,0\,0\,1)$-Zn face and $(0\,0\,0\,\bar{1})$-O face is completely in agreement with the result of the photoemission spectra for a hydrothermal ZnO crystal at about 1.15 [32]. The method provides an effective identification to compare the experimental data with the simplified model. Moreover, the method can quickly point out the trend or condition that belongs to the Zn-rich or O-rich phase on the surface.

5. Conclusion

This study on the proposed simulation of the Auger signal based on the hard-sphere model and the IMFP and EAL database aims to predict the possible received Auger signal. According to our statistical analysis, the results fit well with the experimental ratio of the condition, which is sputtered by Ar^+ ions at 1 keV to 2 keV. The model used by the IMFP data is consistent with the result that the maximum frequency occurs at around 0.428. High temperature annealing leads to higher ratios. When the annealed and sputtered data were compared, all ratios exhibited a downward trend after sputtering. Therefore, the surface type is Zn-rich, even on the $(0\,0\,0\,\bar{1})$ O-face surface. Although the sputtering process and annealed condition are dominant to create a different structure, the surface type can be controlled and monitored. Moreover, the surface information of a crystalline composite material can be quickly determined using the proposed method.

Acknowledgements

Authors first thank Prof. Y.H. Lee and Dr. J.C. Lee in Department of Physics, National Cheng Kung University, Taiwan for supporting the ZnO$(0\,0\,0\,1)$ substrate sample. We would also like to thank sincerely the National Science Council of Republic of China and the National Chiayi University for supporting this work under grand numbers NSC 95-2112-M-415-001, NSC 96-2112-M-415-005-MY2, NSC 98-2112-M-415-003-MY3 and NCYU 96T001-06-04-003.

References

[1] Ü. Özgür, Ya.I. Alivov, C. Liu, A. Teke, M.A. Reshchikov, S. Doğan, V. Avrutin, S.-J. Cho, H. Morkoç, Journal of Applied Physics 98 (2005) 041301.
[2] H.Y. Xu, H. Wang, Y.C. Zhang, S. Wang, M.K. Zhu, H. Yan, Crystal Research and Technology 38 (2003) 429.
[3] P.X. Gao, Z.L. Wang, Journal of Applied Physics 97 (2005) 044304.
[4] A.K. Srivastava, Materials Letters 62 (2008) 4296.
[5] L. Pauling, Journal of the American Chemical Society 49 (1927) 765.
[6] O. Madelung, U. Rössler, M. Schulz, Landolt-Börnstein-Group III Condensed Matter, vol. 41B, Springer-Verlag, Berlin, 1999, pp. 1–4.
[7] Y.Z. Zhu, G.D. Chen, H. Ye, A. Walsh, C.Y. Moon, S.-H. Wei, Physical Review B 77 (2008) 245209.
[8] X. Gu, S. Sabuktagin, A. Teke, D. Johnstone, H. Morkoç, B. Nemeth, J. Nause, Journal of Materials Science: Materials in Electronics 15 (2004) 373.
[9] S. Valeri, S. Altieri, A. di Bona, C. Giovanardi, T.S. Moia, Thin Solid Films 400 (2001) 16.
[10] R. Kosiba, J. Liday, G. Ecke, O. Ambacher, J. Breza, P. Vogrinčič, Vacuum 80 (2006) 990.
[11] H. Kato, M. Sano, K. Miyamoto, T. Yao, Journal of Crystal Growth 265 (2004) 375.
[12] K. Maeda, M. Sato, I. Niikura, T. Fukuda, Semiconductor Science and Technology 20 (2005) S49.
[13] G. Perillat-Merceroz, R. Thierry, P-H. Jouneau, P. Ferret, G. Feuillet, Nanotechnology 23 (2012) 125702.
[14] F. Hamdani, A. Botchkarev, W. Kim, H. Morkoç, M.M. Yeadon, J.M. Gibson, S.-C.Y. Tsen, D.J. Smith, D.C. Reynolds, D.C. Look, K. Evans, C.W. Litton, W.C. Mitchel, P. Hemenger, Applied Physics Letters 70 (1997) 467.
[15] V. Martinelli, L. Siller, M.G. Betti, C. Mariani, U. del Pennino, Surface Science 391 (1997) 73.
[16] A. Sulyok, M. Menyhard, J.B. Malherbe, Surface Science 601 (2007) 1857.
[17] D. Briggs, M.P. Seah (Eds.), Pratical Surface Analysis, Auger & X-ray Photoelectron Spectroscopy, vol. 1, 2nd Ed., Wiley, Chichester, 1990, ch.1, p.6 & ch.5, pp. 244–245.
[18] P. Mazur, S. Zuber, M. Grodzicki, A. Ciszewski, Materials Science-Poland 26 (2008) 265.
[19] C.J. Powell, A. Jablonski, NIST Electron Inelastic-Mean-Free-Path Database Program-Ver.1.1, National Institute of Standards and Technology, Gaithersburg, MD, 2000.
[20] C.J. Powell, A. Jablonski, NIST Electron Effective-Attenuation-Length Database-Ver.1.1, National Institute of Standards and Technology, Gaithersburg, MD, 2003.
[21] R.D. Shannon, Acta Crystallographica Section A 32 (1976) 751.
[22] J.H. Lai, S.H. Su, H.-H. Chen, J.C.A. Huang, C.-L. Wu, Physical Review B 82 (2010) 155406.
[23] H.S. Hsu, J.C.A. Huang, S.F. Chen, C.P. Liu, Applied Physics Letters 90 (2007) 102506.
[24] W.G. Xie, F.Y. Xie, X.L. Yu, K. Xue, J.B. Xu, Applied Physics Letters 95 (2009) 262506.
[25] N. Akdoğan, B. Rameev, S. Güler, O. Öztürk, B. Aktaş, Applied Physics Letters 95 (2009) 102502.
[26] L.E. Davis, N.C. MacDonald, P.W. Palmberg, G.E. Riach, R.E. Weber, Handbook of Auger Electron Spectroscopy, Physical Electronics, Minnesota, 1976.
[27] S. Tanuma, C.J. Powell, D.R. Penn, Surface and Interface Analysis 21 (1994) 165.
[28] W.H. Gries, Surface and Interface Analysis 24 (1996) 38.
[29] Technical report from the Semiwafer Co.ltd, Hsin-Chu, Taiwan, ROC.
[30] X. Zhao, Q. Li, Q. Shi, S. Xue, Z. Li, Y. Liu, Micro and Nano Letters 7 (596) (2012).
[31] J.F. Ziegler, J.P. Biersack, U. Littmark, SRIM V The Stopping and Range of Ions in Matter-SRIM, Pergamon Press, New York, 2009.
[32] N. Ohashi, Y. Adachi, T. Ohsawa, K. Matsumoto, I. Sakaguchi, H. Haneda, S. Ueda, H. Yoshikawa, K. Kobayashi, Applied Physics Letters 94 (2009) 122102.